Autonomous, Additively Manufactured, Multi-Langmuir Probe for CubeSat Plasma Diagnostics

Zoey Bigelow and Luis Fernando Velásquez-García, *Senior Member, IEEE*

***Abstract*— We report the design, fabrication, and characterization of a novel, compact, and fully additively manufactured multi-Langmuir probe (MLP) for CubeSat ionospheric plasma diagnostics. The MLP incorporates three different Langmuir probe (LP) arrangements (i.e., single, dual, and triple LPs) to accurately measure a wide range of plasma properties with redundancy. The reported MLP has integrated low-power, compact electronics and is manufactured using rapid prototyping techniques; consequently, it is a plasma sensing solution compatible with CubeSats that aligns with in-space manufacturing. The dielectric parts of the MLP are made via vat photopolymerization of vitrolite, while the conductive parts of the MLP are made via binder jetting of SS 316L. The electronics of the MLP were verified using calibrated equipment. Experimental characterization of MLP prototypes was conducted using a laboratory helicon plasma chamber, showing good agreement across different LP configurations. The MLP is the first of its kind, enables the implementation of superior and more affordable CubeSat plasma sensors, and aims at providing crucial data to improve our understanding of ionospheric plasma and its implications for climate change.**

***Index Terms*— 3-D printed CubeSat instrumentation, binder jetting, glass-ceramic vat photopolymerization, Langmuir probes (LPs), plasma diagnostics.**

I. Introduction

THE ionosphere is a critical layer of the Earth's atmosphere that is composed entirely of plasma—a quasi-neutral, superheated state of matter consisting of neutral molecules, ions, and electrons [1]. Of great scientific interest is the thermosphere, a region within the ionosphere extending approximately 80–600 km above Earth's surface that plays a significant role in global warming [2]. However, obtaining accurate plasma measurements in this region has proven challenging. While plasma measurements of the thermosphere can be taken from afar (from the Earth's surface or with satellites in orbit), the most reliable data are gathered by satellites orbiting within the thermosphere [3]. Given the high cost associated with launching hardware into space, the use of CubeSats is an ideal solution to collect ionospheric plasma data [4], [5]. Consequently, there is a strong demand for low-cost and compact plasma diagnostic instrumentation that can be directly integrated into CubeSats.

Langmuir probes (LPs) are plasma sensors known for their simplicity, versatility, and minimal maintenance requirements, which makes them an excellent choice as plasma instrumentation onboard CubeSats [6]. Moreover, the utilization of rapid prototyping techniques enables their swift and cost-effective manufacturing, with minimal waste, even in space. Three common LP configurations involve single, dual, and triple probe arrangements, each offering distinct advantages and limitations. Among these configurations, the single LP setup is the simplest, serving as a straightforward LP sensor design. In contrast, dual LPs offer the advantage of drawing less current from the plasma compared to single LPs, resulting in lower plasma perturbation and more accurate measurements [7]. Triple LPs, on the other hand, provide faster measurements of plasma parameters. However, they are only suitable for cases where the plasma can be assumed to have a Maxwellian distribution (a statistical distribution based on the kinetic theory of gases, where the molecules are in thermal equilibrium; in mathematical terms, it is the chi distribution with three degrees of freedom, where the velocity of the particles is proportional to the square root of the temperature divided by the mass of the particle); furthermore, triple LPs are not well-suited for measuring floating and plasma potentials [8]. Nonetheless, triple LPs excel in capturing instantaneous and time-sensitive plasma measurements, while single and dual LPs are used to extract time-averaged plasma parameters [9]. It would be advantageous to integrate the three types of LP arrangements into a single instrument, closely spaced while running independently, to leverage their strengths and introduce redundancy in the estimation of the plasma parameters to improve the reliability of such estimates.

Numerous studies have implemented and characterized single, dual, and triple LPs [7], [8], [9], [10], including sets of LPs meant to work together to characterize plasma. For instance, Ghosh et al. [11] introduced a design utilizing three

Manuscript received 20 September 2023; revised 3 December 2023; accepted 4 January 2024. Date of publication 4 March 2024; date of current version 14 March 2024. This work was supported in part by the NewSat Project, which is co-funded by the Operational Program for Competitiveness and Internationalization (COMPETE2020), Portugal 2020; in part by European Regional Development Fund (ERDF); and in part by Portuguese Foundation for Science and Technology (FTC) under the MIT Portugal Program. The Associate Editor coordinating the review process was Dr. Ada Fort. *(Corresponding author: Luis Fernando Velásquez-García.)*

Zoey Bigelow is with the Department of Electrical Engineering and Computer Science, Massachusetts Institute of Technology, Cambridge, MA 02139 USA (e-mail: zbigelow@mit.edu).

Luis Fernando Velásquez-García is with Microsystems Technology Laboratories, Research Laboratory of Electronics, Massachusetts Institute of Technology, Cambridge, MA 02139 USA (e-mail: Velasquez@alum.mit.edu).

Digital Object Identifier 10.1109/TIM.2024.3373052

electrodes that can be used as either a dual LP or a triple LP, depending on the users' need to estimate time-sensitive or time-averaged plasma parameters. Jin et al. [12] patented a "three-in-one detection system" with four electrodes capable of running either single, dual, or triple LPs or single and triple LPs simultaneously if so desired. However, to the best of our knowledge, the multi-Langmuir probe (MLP) presented in this study is the first LP design to implement all three of the configurations to be used simultaneously. Despite recent reports of 3-D printed CubeSat hardware, such as retarding potential analyzers and thrusters [13], [14], to the best of our knowledge, the MLP stands as the first additively manufactured LP sensor. The compact, low-weight, and low-power MLP is manufactured via rapid prototyping techniques, establishing a cost-effective solution for CubeSat-based in situ space plasma sensing. Moreover, 3-D printing's compatibility with in-space manufacturing by creating net-shape objects and by utilizing multipurpose feedstock to minimize waste addresses the substantial expenses associated with launching payloads into space [4].

This study presents the design, fabrication, and characterization of a novel, additively manufactured, compact MLP for CubeSat plasma diagnostics. Section II describes the design of the MLP. In Section III, the manufacturing process of the MLP is detailed, including the characterization of the 3-D printed ceramic housing, the 3-D printed electrodes, and the circuitry developed to run the entire device. In Section IV, the characterization of the MLP is presented. Section V discusses the results and suggests tentative directions for future research, while Section VI concludes the work.

II. Proposed System Design

This section reports the overall structure of the MLP, the underlying physical principle of its operation, and the specifications of the MLP designs explored in this study. A key aspect in the MLP's design process entailed the development of low-power, compact, integrated circuitry that enables the entire device to operate autonomously without any other support equipment or instrumentation, at power levels compatible with those available on a typical CubeSat.

A. Principles of Operation of LPs

LPs are, fundamentally, electrodes [typically made of tungsten or stainless steel (SS)] that are biased at a specific voltage and immersed in a plasma environment. LPs are shielded by a dielectric jacket (typically made of ceramic, e.g., alumina, or a polymer, e.g., polyamide), except at their tip. The dielectric shielding improves the structural rigidity of the LP, and it also allows LPs to be inserted farther into the plasma to conduct localized measurements while minimizing plasma perturbation. LPs attract free-floating charged particles that are registered as current through the electrodes; the current is measured and used to estimate plasma properties. In the case of the single LP configuration, a range of bias voltages is swept (a ±100-V voltage range is typically employed for LPs intended for electric propulsion diagnostics [8], while a ±10-V voltage range is typically used in LPs for ionospheric studies [6]), varying from negative to positive relative to a common reference point, such as the vacuum chamber (on-ground operation) or the spacecraft frame (in-space operation). The measured currents (which can range from microampere level or less to milliampere level or more, depending on the plasma and the dimensions of the exposed tip of the LP) can be plotted against the applied bias voltage to produce an I–V characteristic that is analyzed to extract various plasma properties (see Fig. 1). The plasma potential, V_p, is the potential at which the electron saturation current occurs, while the floating potential, V_f, is the potential at which the measured current is zero. For a large enough bias voltage, the current in the electrode saturates and is mostly composed of either electrons (positive bias voltage) or ions (negative bias voltage); these are called the electron and ion saturation currents, respectively. The electron temperature, T_{eV}, is one of the simpler parameters to find from the I–V characteristic of a single LP. If the plasma is Maxwellian, the exponential portion on the I–V characteristic is proportional to $\exp(-V/T_{\mathrm{eV}})$; therefore, the slope of the logarithm of the current versus voltage curve is a constant proportional to the inverse of the temperature T_{eV} [8]. Single LPs often experience a phenomenon known as sheath expansion [15]; as the bias voltage becomes very large, the sheath expands, creating a larger collection area that allows for more electrons to be captured, which in turn increases the sheath thickness. This feedback loop results in the electron saturation current region becoming exponential rather than constant. Consequently, to keep the measured currents low, single LP data are typically collected from very negative bias voltages to moderately positive bias voltages.

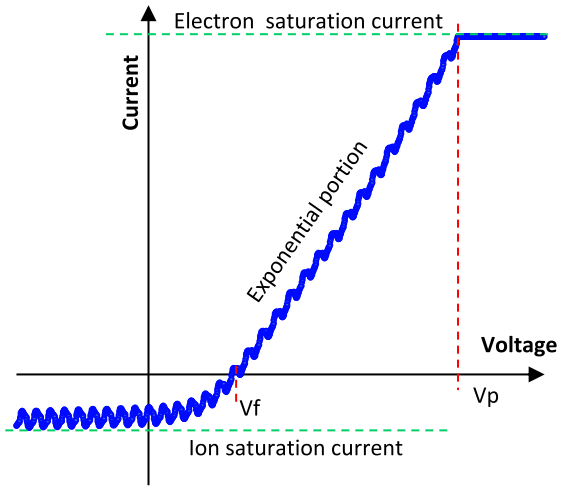

Fig. 1. Schematic of a single LP I–V characteristic with its key parameters indicated.

Dual LPs function similar to single LPs, but the bias voltage swept on one electrode is referenced to the second electrode, which is floating. Given that the reference of the LP can shift with the floating electrode, sheath expansion is no longer a possibility; therefore, the analysis of the I–V characteristic of a dual LP (see Fig. 2) changes slightly. The floating potential is still given by the bias voltage at which the measured current

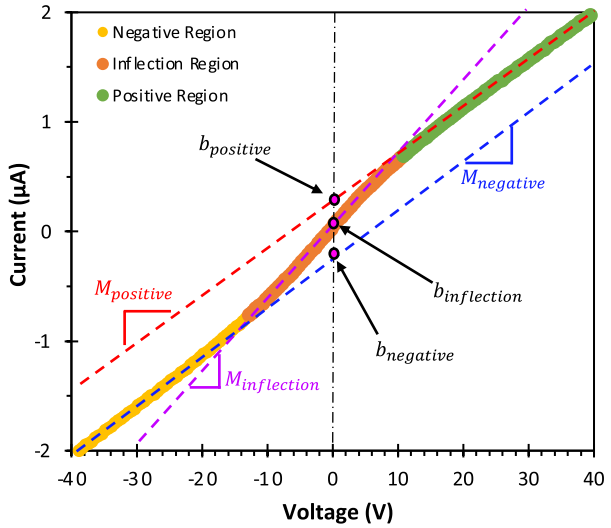

Fig. 2. Schematic of a dual LP I–V characteristic with key regions indicated.

is zero. The linear fits of the three regions (negative region—dominated by ions; positive region—dominated by electrons; inflection region) give three slopes (M_{negative}, M_{positive}, and $M_{\text{inflection}}$, respectively) and three y-intercepts (b_{negative}, b_{positive}, and $b_{\text{inflection}}$, respectively). The electron temperature (in electronvolt), T_{eV}, is found from the linear fits of all three regions via [16]

$$T_{\text{eV}} = \frac{b_{\text{positive}} - b_{\text{negative}}}{4\left(1.08M_{\text{inflection}} - 0.79M_{\text{positive}}\right)} \tag{1}$$

where the constant coefficients are found from the equivalent resistance method developed by Chang and Laframboise [17]. Experimentally, V_p can be estimated from the intersection of the inflection and positive regions; a theoretical, approximate value can be found from V_f and T_{eV} [18] through the expression

$$V_p = V_f + 0.5T_{\text{eV}} \ln\left(\frac{2m_i}{\pi m_e}\right) \tag{2}$$

where m_e and m_i are the masses of an electron and of an ion, respectively.

The values found directly from the I–V characteristics of the single and dual LPs can be used to find other plasma parameters. An important parameter that strongly influences the behavior of the LP is the Debye length, λ_D. The Debye length is the distance that an electrostatic field penetrates a plasma and is specific to a given plasma [6]. The Debye length is given by

$$\lambda_D = \sqrt{\frac{\varepsilon_0 T_{\text{eV}}}{n \cdot e}} \tag{3}$$

where ε_0 is the permittivity of free space, n is the number density, and e is the electron's charge. It is vital to maintain a separation distance of at least twice the Debye length to prevent interference between adjacent electrodes. Additionally, the interaction between the plasma and the electrodes depends on the size of the probe's radius relative to the Debye length. Specifically, the ratio r_P/λ_D, where r_P is the electrode radius, defines to what extent radio frequency (RF) effects need to be

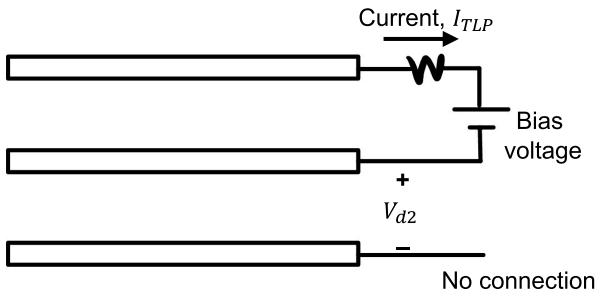

Fig. 3. Schematic of a triple LP.

compensated for and determines the applicable equations for calculating the number density [8].

The equations governing plasma–LP interactions can be derived from the equations of motion, Boltzmann's relation, and the principle of quasi-neutrality, which states that the number density of ions and electrons is approximately equal [8]. Using these, it is found that when r_P/λ_D is larger than 50, the plasma sheath is thin enough to be negligible (called the "thin sheath-limit"); in such case, the number density, n, is given by

$$n = -\frac{I_{\text{is}}}{\exp(-0.5)eA}\sqrt{\frac{m_i}{eT_{\text{eV}}}} \tag{4}$$

where A is the surface area of the electrode exposed to the plasma. Given that Debye lengths inherent to the ionosphere are much larger than those in laboratory plasmas, an MLP system designed for the ionosphere is fully capable of also characterizing laboratory plasmas.

Triple LPs do not implement a voltage sweep to measure currents to infer plasma parameters. Instead, two of the electrodes are set to a voltage differential with reference to the third electrode, making this the only configuration that makes real-time plasma measurements [9]. A triple LP makes two measurements, i.e., the current flowing through the biased electrode, I_{TLP}, and the potential difference between the biased electrode and the floating electrode, V_{d2} (see Fig. 3). The applied voltage differential should be between five and ten times the anticipated value of V_{d2}; when this requirement is satisfied, I_{TLP} is equal to the ion saturation current [11]. The electron temperature is related linearly to V_{d2} as

$$T_{\text{eV}} = \frac{-V_{d2}}{\ln(0.5)} \tag{5}$$

Triple LPs are unique in that the value of V_{d2} accounts for sheath expansion, as well as the effects of the ratio r_P/λ_D. Therefore, a single equation that considers V_{d2} can be used in calculating the number density, regardless of whether the LP is operating in the thin sheath limit [9]. Consequently, n in a triple LP is found via

$$n = \frac{I_{\text{TLP}}}{Ae\sqrt{\frac{eT_{\text{eV}}}{m_i}}} \frac{\exp\left(-\frac{V_{d2}}{T_{\text{eV}}}\right)}{1 - \exp\left(-\frac{V_{d2}}{T_{\text{eV}}}\right)} \tag{6}$$

The plasma parameters that can be found using single, dual, and triple LPs are summarized in Table I.

These plasma parameters will shift their values as the plasma itself changes. For example, helicon plasmas are

TABLE I
PLASMA PARAMETERS THAT CAN BE INFERRED FROM DATA COLLECTED USING SINGLE, DUAL, AND TRIPLE LPS

Parameter (units)	Description	LP Configuration Used
Plasma potential V_p (V)	Potential inherent in the plasma itself	Single, dual
Floating potential V_f (V)	Potential inherent in the sheath surrounding the electrode	Single, dual
Electron temperature T_{ev} (eV)	Temperature of the plasma	Single, dual, and triple
Ion saturation current I_i (A)	Current at which the maximum number of ions per unit of time strike the electrode	Single, dual, and triple
Electron saturation current I_e (A)	Current at which the maximum number of electrons per unit of time impact the electrode	Single, dual
Number density n (m^{-3})	Number of particles per unit of volume	Single, dual, and triple
Debye length λ_D (m)	Distance that an electrostatic field penetrates a plasma	Single, dual, and triple

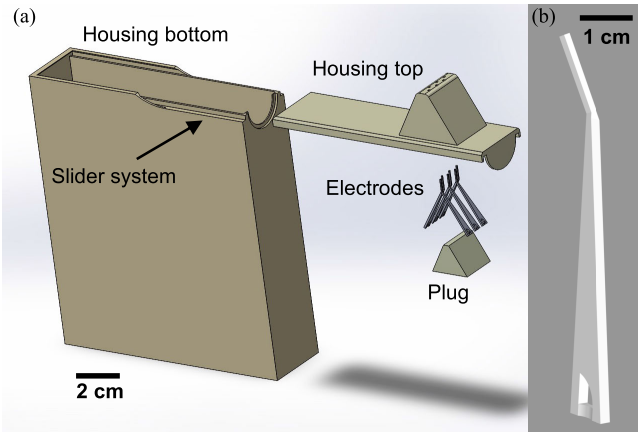

Fig. 4. (a) Computer-aided design (CAD) exploded view of an MLP. The driving electronics are inside the housing bottom. The housing top and bottom are assembled using a slider mechanism. (b) CAD close-up of an LP electrode used in the MLP.

created by applying an RF signal to a gas, causing the gas to ionize and become a plasma. The number density of the plasma, n, will increase with the RF power [16]. Similarly, the electron temperature, T_{eV}, will increase slightly with RF power, but to a much lesser degree than n [18]. This difference determines how the Debye length, λ_D, varies with RF power. Given that n has a stronger dependence on RF power than T_{eV}, λ_D decreases as RF power increases. Other relevant parameters include the floating potential, which increases slightly with RF power, and the plasma potential, which typically remains stable [18].

B. Proposed MLP Structure

The MLP consists of three distinct components: electrodes, circuitry, and housing (see Fig. 4), facilitating the implementation of the three independent LP configurations (single, dual, and triple). These probes operate concurrently, enabling redundant plasma parameter estimation.

In the MLP, the electrode's separation is crucial: the electrodes should be as close together as possible to attain local plasma measurements, yet far enough apart that there is no interference between adjacent electrodes. The electrodes used in this study [see Fig. 4(b)] have a 0.5 × 0.5 mm tip cross section, which is standard in the LP literature [16] and about the smallest as-printed features that can be reliably defined with mainstream metal 3-D printing techniques. By utilizing a 30° angle at the point where the electrode begins to widen, the tips of the electrodes are brought close together at the sensing end of the electrode, while the bulkier parts of the electrodes are spaced apart and more robustly anchored. In the MLP, the electrodes were widened linearly to 3 mm. The six electrodes required to run the three LP configurations are named SLP1, DLP1, DLP2, TLP1, TLP2, and TLP3, where the letters denote whether the electrode is part of a single, dual, or triple LP configuration and the number denotes which electrode of the configuration it belongs to.

The housing of the MLP fulfilled two requirements: 1) holding the electrodes securely in place and 2) protecting the circuitry from the plasma environment. Previous experiments with the laboratory plasma used to characterize the MLP showed the plasma generated by the helicon source had associated Debye lengths as large as 100 μm [13], i.e., the MLP electrodes needed to be at least 200 μm apart to avoid interference. In contrast, plasmas in the ionosphere have much larger Debye lengths, approximately 1 mm [6]. Therefore, two housing tops were developed: a top with an electrode spacing of 300 μm that pushed the lower bound of separation and fabrication precision available for the MLP study [see Fig. 5(a)] and a top with an electrode spacing of 5 mm that could operate in the ionosphere as well as accommodate a wider range of laboratory plasma densities [see Fig. 5(b)]. The tops are easily interchangeable via a slider mechanism that attaches them to the bottom housing base. The hole at the bottom of the housing that allows the device to be plugged in also offers a sufficient gap for ventilation, thereby preventing air becoming trapped inside the MLP.

The MLP circuitry requirements (see Table II) were achieved using Arduino[1] Nano 33 internet of things (IoT) modules, MAX629 boost converter chips, an array of operational amplifiers (op amps), and difference amplifiers (see Table III). The Arduino[1] modules, which are often used on CubeSats [19], [20], [21], [22], [23], provided the initial varying bias voltage signal of 0–3.3 V (the full voltage range of these kind of devices) at a period of 5.5 s and a measure count of 1022 for the single and dual LPs. This period enabled the voltage sweep to occur slowly enough that the signal was quasistatic, i.e., it was a dc voltage step signal, as opposed to an ac sawtooth signal. When an ac signal is applied to LPs, the parallel electrodes behave like a capacitor. While it is possible to add circuit elements to correct this issue [7],

[1]Registered Trademark.

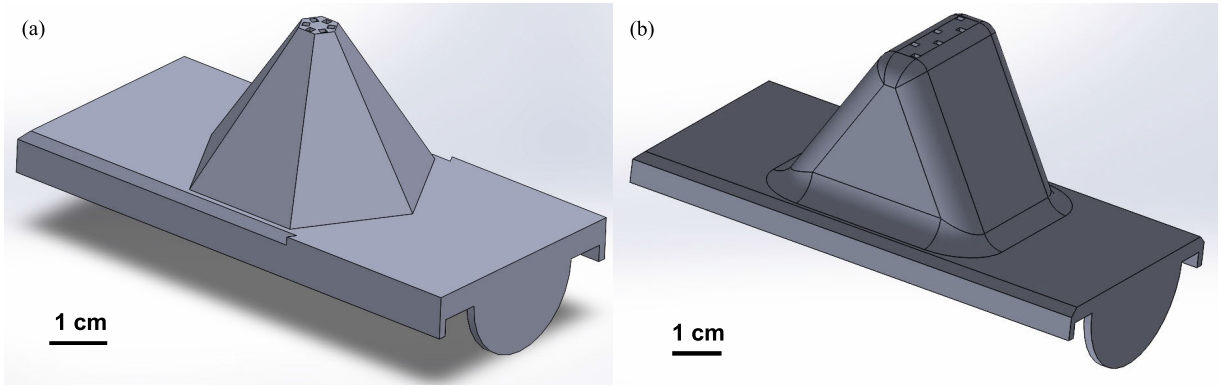

Fig. 5. CAD model of the housing top with (a) minimal electrode spacing (i.e., 300 μm) and (b) lower bound spacing for ionospheric plasma (i.e., 5 mm).

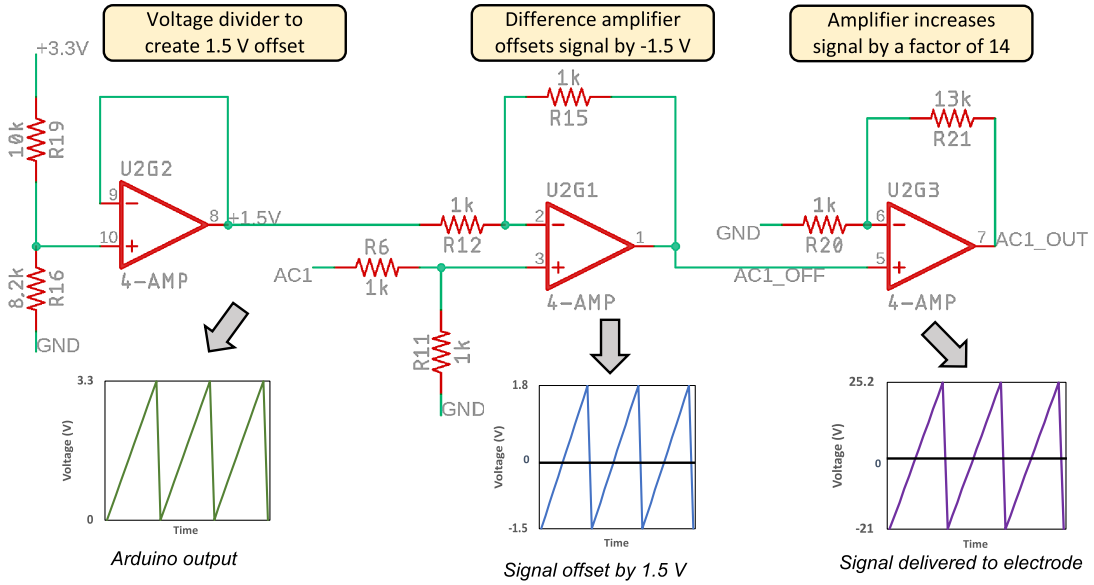

Fig. 6. Circuit schematic between Arduino[1] module and electrode tip with insets of the output at different points of the circuit.

TABLE II
MLP ELECTRONICS REQUIREMENTS TO RUN SINGLE, DUAL, AND TRIPLE LPS SIMULTANEOUSLY

Probe	Function
Single LP (output)	Sweep from -20 V to 25 V in 3.2 mV steps (with reference to ground)
Single LP (input)	Measure current through SLP1
Dual LP (output)	Sweep from -20 V to 25 V in 3.2 mV steps (with reference to DLP1)
Dual LP (input)	Measure current through DLP2
Triple LP (output)	Apply 25 V to TLP1 (with reference to TLP3)
Triple LP (input 1)	Measure current through TLP1 (i.e., I_{TLP})
Triple LP (input 2)	Measure potential difference between TLP1 and TLP2 (i.e., V_{d2})

TABLE III
REFERENCE SHEET FOR MLP CIRCUIT COMPONENTS

Component	Reference Number
Arduino® modules	Arduino® Nano 33 IoT
Boost converters	MAX629
Operational amplifiers	ADA4522-4
Difference amplifiers	ADA629

keeping the sweep frequency low avoided the issue entirely. These signals were then centered and amplified using the op amp array. The op amps were powered using MAX629 boost converter chips to achieve the necessary bias voltage range (~45 Vpp). The transformation of the bias voltage sweeps for the single and dual LPs going from the Arduino[1] modules to the electrodes is depicted in Fig. 6. Past tests in this plasma source resulted in V_{d2} values between 3 and 5 V; therefore, a dc bias voltage of 25 V was chosen for the triple LP, which was also produced by the MAX629 chips. The input currents were measured using difference amplifiers, which measured the voltage drop across a shunt resistor and then fed that signal into one of the Arduino[1] modules. According to LP theory, current can be measured with LPs applying bias voltage signals as high as 1 MHz per sample [7]. Given that the MLP signal was orders of magnitude slower, measuring the current values quickly enough was not an

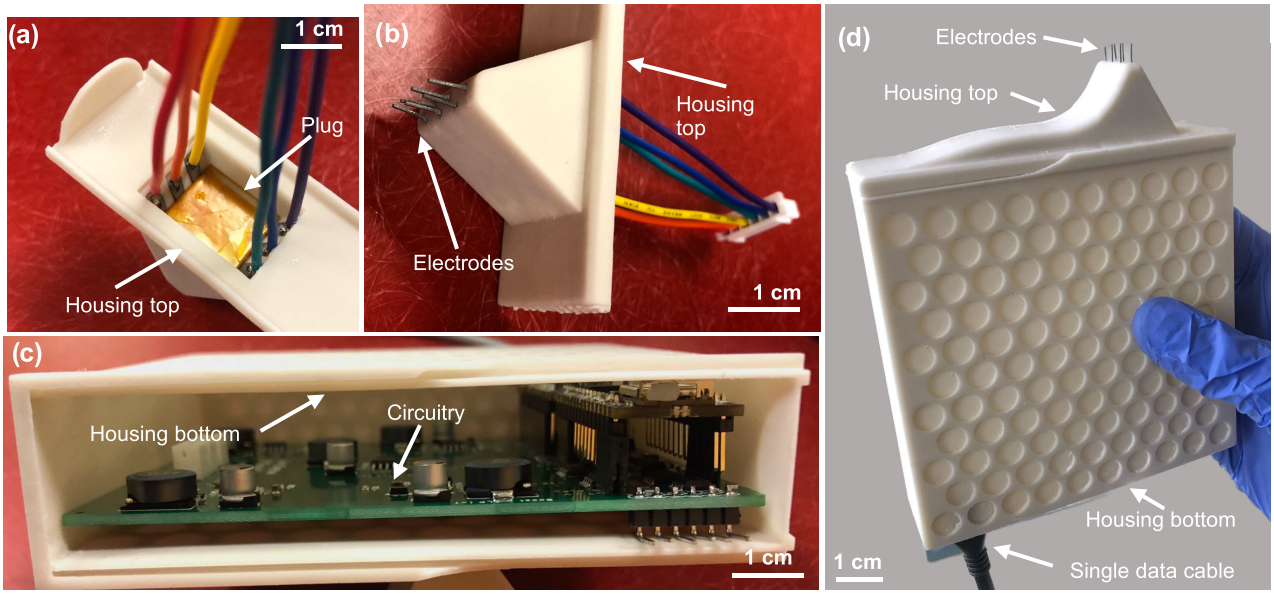

Fig. 7. Selected images of an MLP during assembly. (a) Underside of the housing top showing the plug holding the electrodes in place. (b) Top side of the housing top showing the array of electrodes protruding. (c) Housing bottom with the driving circuit inside. (d) Fully assembled device.

issue. By using rechargeable lithium-polymer batteries in the design, the entire device was able to be run using a single micro-USB B cable.

The final dimensions of the MLP housing bottom were $10.2 \times 10.2 \times 2.8$ cm (0.29 L), while the tip of the housing top protruded an additional 2.3 cm. The electrodes were positioned to protrude 3 mm out of the housing top. The walls of the housing are 2.5 mm thick to minimize material while still being structurally sufficient. The assembled MLP weighs 300 g, resulting in a mass density about a quarter lower than the 1.3 kg/L limit for a CubeSat.

III. Device Fabrication

Compared to traditional manufacturing methods, 3-D printing is better suited for in-space manufacturing due to its ability to employ multipurpose feedstock, customize the designs, and produce less waste. Nonetheless, additive manufacturing poses some disadvantages compared to traditional manufacturing. For example, mainstream additive manufacturing methods are not as precise. Also, the properties of the printed material could be lesser (e.g., mechanically weaker, less chemically resistant, less vacuum compatible), which in some cases stem as tradeoff of the material printability and in other cases is related to the orientation of the printed layers. More information is found elsewhere [24]. The electrodes used in LPs are typically constructed from wires made of high-temperature compatible materials, such as SS or tungsten [8], [16], [25]; while 3-D printing of tungsten is in its infancy, 3-D printing methods for SS are mature and some of them have adequate resolution to implement finely featured objects [26]. SS 316L was chosen as the material for the MLP electrodes due to its material properties (high electrical conductivity, high yield stress, high temperature compatibility, and low vacuum outgassing [26]), as well as the accessibility and maturity of its 3-D printing process [27]. The electrodes were fabricated via binder jetting (a printing method that decouples the printing of the object and its consolidation, greatly increasing the precision of the printed objects) by the vendor iMaterialise (Leuven, Belgium). Binder jetting is known for its low residual stresses and high resolution, as it decouples the printing and consolidation of the object [26]. Given the prevalence of oxygen in the ionosphere [4], the electrodes should be coated with a low-oxidizing material to avoid chemical degradation because electrode degradation results in diminished surface conductivity, reduced current collection, and less accurate I–V characteristics [28]. While gold is the most-used coating for LP electrodes [29], a study by Samaniego and colleagues [25] found that iridium outperforms the other materials tested, including gold, in highly oxidizing environments. Therefore, the electrodes were sputter-coated with a conformal, 20-nm-thick iridium film.

The choice of material for the housing was primarily driven by the need to provide a secure, electrically insulating physical enclosure for the electrodes and electronics, while also exhibiting the capability to withstand elevated temperatures without profusely outgassing in vacuum. Unlike other printing methods for ceramics, vat photopolymerization does not produce coarse, porous objects incompatible with vacuum applications [30]. For these reasons, the housing was 3-D printed via vat photopolymerization in vitrolite using a Bison 1000 3-D printer (Tethon3D, Omaha, Nebraska, USA). This printer utilizes a digital light processing (DLP) engine that employs a 1920×1080 array of 405-nm UV LED pixels, with each pixel measuring 57 μm. The Bison 1000 employs a heating mechanism to warm up the resin in the printer's vat, reducing its viscosity and improving the adhesion of the printed part to the printer platform. Additionally, the printer is housed within a custom HEPA filtered cabinet, ensuring a controllable, clean workspace. Given our previous experience with vacuum compatible devices 3-D

TABLE IV
PEAK OPERATING VOLTAGE, PEAK MEASURED CURRENT, AND POWER CONSUMPTION FOR EACH LP CONFIGURATION WITHIN THE MLP

Configuration	Peak Operating Voltage (V)	Peak Measured Current (mA)	Power Consumption (mW)
Single LP	5.0 V	73.2	366
Dual LP	7.4 V	55.4	410
Triple LP	3.7 V	2.7	10
Total			**786**

printed in vitrolite via vat photopolymerization [13], the printed pieces were used in their green state, i.e., without sintering, which ensured the tightest dimensional tolerances. To decrease material use, circular cutouts with hexagonal packing were implemented in the body of the housing bottom.

The assembly of the MLP is conducted in three distinct stages (see Fig. 7). First, the electrodes are placed in the housing top and secured into place using a ceramic plug [see Fig. 7(a) and (b)]. Then, the circuit is placed in the housing bottom [see Fig. 7(c)]. Finally, the top housing piece is slid into place [see Fig. 7(d)].

IV. EXPERIMENTAL DEVICE CHARACTERIZATION

This section reports the characterization of the MLP, including 1) experimental characterization of the driving circuit without plasma and 2) experimental characterization of the MLP using a helicon plasma source.

A. Experimental Characterization of the MLP Driving Circuitry

LPs work simply by applying a voltage and measuring a resulting current drawn from a plasma; from those measurements, plasma properties are inferred. Therefore, benchmarking the electronics of a plasma sensor using calibrated equipment is sufficient for ensuring their correct operation [31]. Consequently, thorough testing was done for the various parts of the circuit before conducting plasma tests to ensure the validity of any subsequent measurements made in the plasma. The dc voltages were measured using a Fluke[1] 28II True rms Multimeter (Fluke Corporation, Everett, WA, USA), while other signals were measured using a Rigol[1] DS6104 Digital Oscilloscope (Rigol, Portland, OR, USA).

The power consumption of the MLP was estimated using the superposition technique, which involves considering the contribution of each source or element in isolation. To do this, a Rigol[1] DP832A Programmable dc power supply was used to activate only one input at a time (e.g., power for Arduino[1] modules, battery for the triple boost converter) and to measure the current each input drew, while the rest of the circuit remained inactive. In this way, the power consumption of each LP configuration was evaluated (see Table IV). The total power consumption of the device is estimated at 786 mW, which is well within the range of power that a typical CubeSat can supply [32].

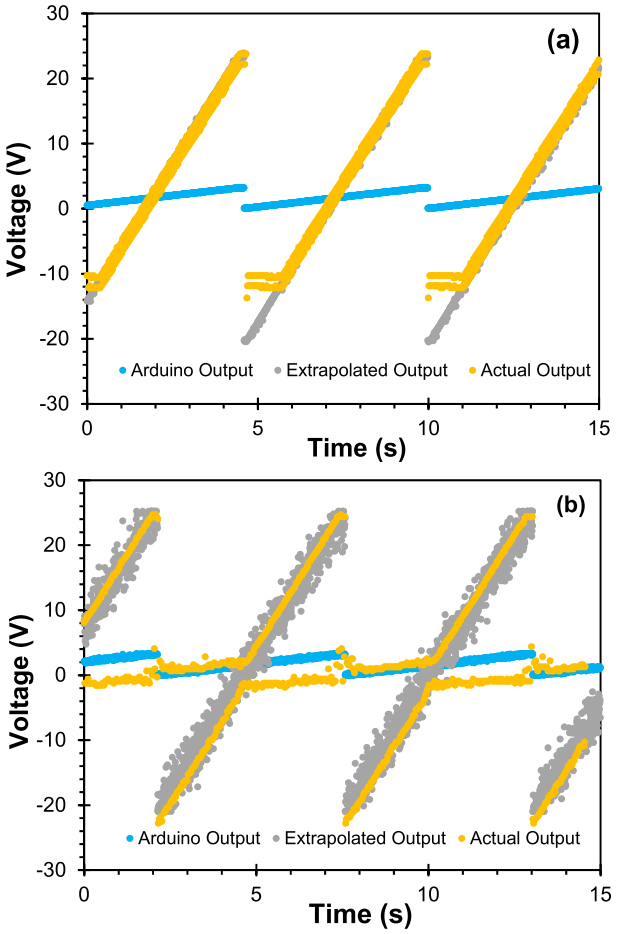

Fig. 8. Voltage sweeps for (a) single and (b) dual LPs showing the outputs from their respective Arduino[1] modules, the extrapolated outputs based on (7), and the actual signal outputs from their respective output electrodes.

To verify the circuit's capability to drive the MLP, different sections responsible for powering the single, dual, and triple LPs were individually tested. This involved testing the voltage sweep for the single [see Fig. 8(a)] and dual LPs [see Fig. 8(b)], as well as the dc output for the triple LP. Due to the Arduino[1] module's inability to measure the actual output of the single and dual LPs, the initial 0–3.3-V outputs were measured separately for each of the two configurations, and the resulting signals were extrapolated using the following equation, which accounts for the amplification of the signals caused by the op amp system (as shown in Fig. 6):

$$V_{\text{out}} = (V_{\text{Arduino}} - 1.5\ \text{V}) \cdot 14 \tag{7}$$

where 1.5 V is the offset and 14 is the gain. Ideally, the actual output and the extrapolated signals shown in Fig. 8 would be identical. In the case of the single LP circuit, there is a slight cutoff around −10 V. This is attributed to the negative boost converter operating below peak efficiency due to the load on the rest of the circuit. However, this does not affect the overall collection of plasma data, as a sweep as low as −10 V is sufficient to capture a reliable single LP I–V characteristic. Although the output signal for the dual LP exhibits 8.5% more noise than the output signal of the single LP, it reaches the full

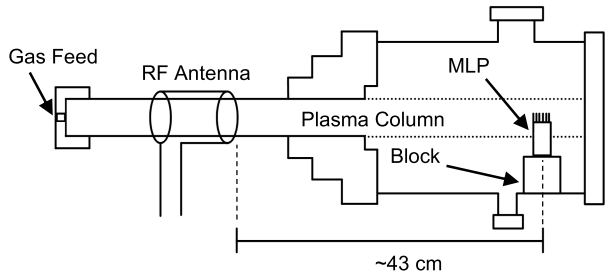

Fig. 9. Diagram of the helicon plasma source used to characterize the MLP.

TABLE V
POLYNOMIAL FIT COEFFICIENTS FOR SINGLE LP *I–V* CHARACTERISTICS

Power Level	Polynomial Fit Coefficients ($y=ax^7+bx^6+cx^5+dx^4+ex^3+fx^2+gx+h$)
100 W	$a=-8.6\times10^{-9}$, b $=7.7\times10^{-8}$, c $=6.4\times10^{-6}$, d $=-8.9\times10^{-5}$, e $=-4.4\times10^{-4}$, f $=9.1\times10^{-2}$, g $=1.3$, h $=4.4$
200 W	$a=1.4\times10^{-10}$, $b=5.4\times10^{-8}$, $c=-2.4\times10^{-6}$, $d=-9.4\times10^{-5}$, $e=2.7\times10^{-3}$, $f=1.2\times10^{-1}$, $g=1.3$, $h=4.575$
300 W	$a=-6.5\times10^{-8}$, $b=4.4\times10^{-7}$, $c=6.0\times10^{-5}$, $d=-2.3\times10^{-3}$, $e=-1.5\times10^{-2}$, $f=9.3\times10^{-2}$, $g=2.7$, $h=8.5$
400 W	$a=-1.0\times10^{-7}$, $b=2.0\times10^{-6}$, $c=9.1\times10^{-5}$, $d=-1.3\times10^{-3}$, $e=-2.7\times10^{-2}$, $f=2.9\times10^{-1}$, $g=4.4$, $h=8.7$
500 W	$a=3.6\times10^{-9}$, $b=-4.5\times10^{-7}$, $c=-1.3\times10^{-5}$, $d=1.7\times10^{-4}$, $e=8.2\times10^{-3}$, $f=1.2\times10^{-1}$, $g=1.2$, $h=5.1$

range of the voltage sweep. The additional noise is likely due to the difference amplifier used to measure the floating dual LP voltage output with reference to ground. The expected dc output for the triple LP was 24.6 V. It was measured at 25.6 V, resulting in a difference of 4%.

B. Experimental Characterization of the MLP Using a Helicon Plasma Source

The MLP was tested using a helicon plasma source at MIT's Plasma Science and Fusion Center (PSFC). This source generates a helicon plasma by exciting gas with a helicon wave. To operate the helicon plasma source, the pressure in the chamber is decreased to 2×10^{-5} Torr. Then, gas (in this case helium) is introduced and excited into a plasma state by a 13.56-MHz RF power source. The plasma used in these tests was not magnetized. More information on the PSFC's helicon plasma source can be found elsewhere [16]. The MLP was installed in the helicon plasma source on a block in the center of the chamber. This way, the LP electrodes were suspended in the center of the plasma, radially, approximately 43 cm from the plasma source (see Fig. 9). To easily control the ON/OFF state of the dual and triple LP batteries, they were replaced by polyether ether ketone (PEEK) cables and connected via feedthroughs to a floating dc power supply outside the plasma chamber. Additionally, the micro-USB B cable was connected to a computer via a feedthrough, enabling real-time data acquisition. The plasma RF power was varied between 100 and 500 W in steps of 100 W. After examination of several fits, it was determined

TABLE VI
POLYNOMIAL FIT COEFFICIENTS FOR DUAL LP *I–V* CHARACTERISTICS

Power Level	Polynomial Fit Coefficients ($y=ax^7+bx^6+cx^5+dx^4+ex^3+fx^2+gx+h$)
100 W	$-a=5.8\times10^{-9}$, $b=-5.4\times10^{-8}$, $c=2.6\times10^{-6}$, $d=2.2\times10^{-5}$, $e=1.2\times10^{-3}$, $f=4.7\times10^{-2}$, $g=5.1\times10^{-1}$, $h=1.6$
200 W	$a=-6.4\times10^{-9}$, $b=-2.3\times10^{-8}$, $c=2.5\times10^{-6}$, $d=-1.4\times10^{-6}$, $e=1.9\times10^{-3}$, $f=6.7\times10^{-2}$, $g=5.7\times10^{-1}$, $h=1.2$
300 W	$a=3.6\times10^{-9}$, $b=-2.7\times10^{-7}$, $c=-8.4\times10^{-6}$, $d=1.8\times10^{-4}$, $e=6.5\times10^{-3}$, $f=5.2\times10^{-2}$, $g=1.1\times10^{-1}$, $h=8.2\times10^{-2}$
400 W	$a=2.7\times10^{-10}$, $b=-2.8\times10^{-7}$, $c=-7.4\times10^{-6}$, $d=1.7\times10^{-4}$, $e=7.3\times10^{-3}$, $f=7.2\times10^{-2}$, $g=1.7\times10^{-1}$, $h=-0.2$
500 W	$a=3.6\times10^{-8}$, $b=-7.3\times10^{-7}$, $c=-4.0\times10^{-5}$, $d=4.4\times10^{-4}$, $e=1.7\times10^{-2}$, $f=5.0\times10^{-2}$, $g=-4.1\times10^{-1}$, $h=-2.1\times10^{-1}$

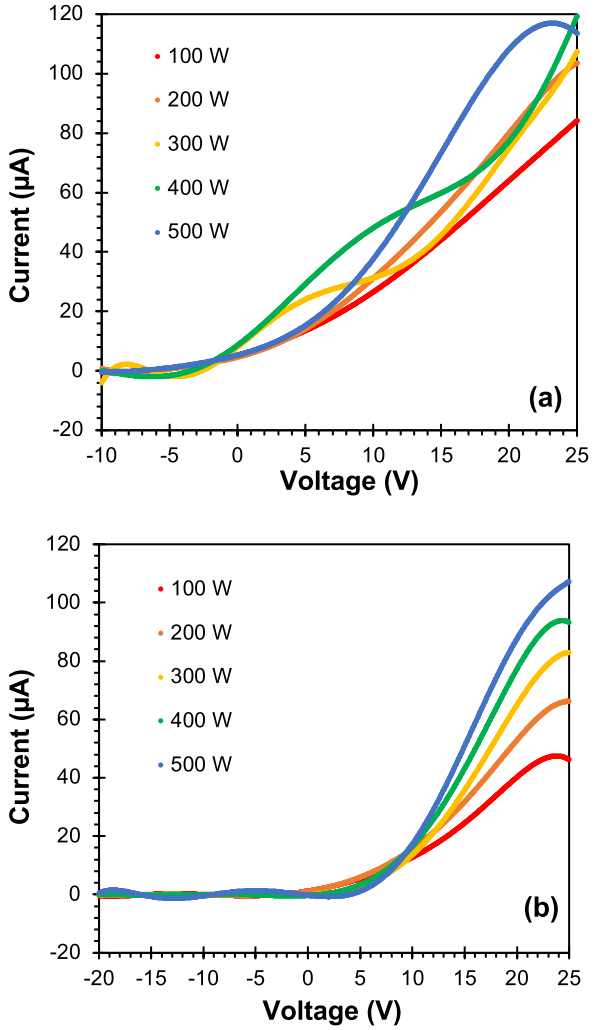

Fig. 10. *I–V* characteristics for five different plasma power levels using the (a) single LP and (b) dual LP.

that a seventh-order polynomial fit the data collected as *I–V* characteristics best (see Tables V and VI). The MLP version tested used the top housing with 5-mm electrode separation (the configuration compatible with both laboratory plasmas and the ionosphere). Fig. 10 shows the *I–V* characteristic

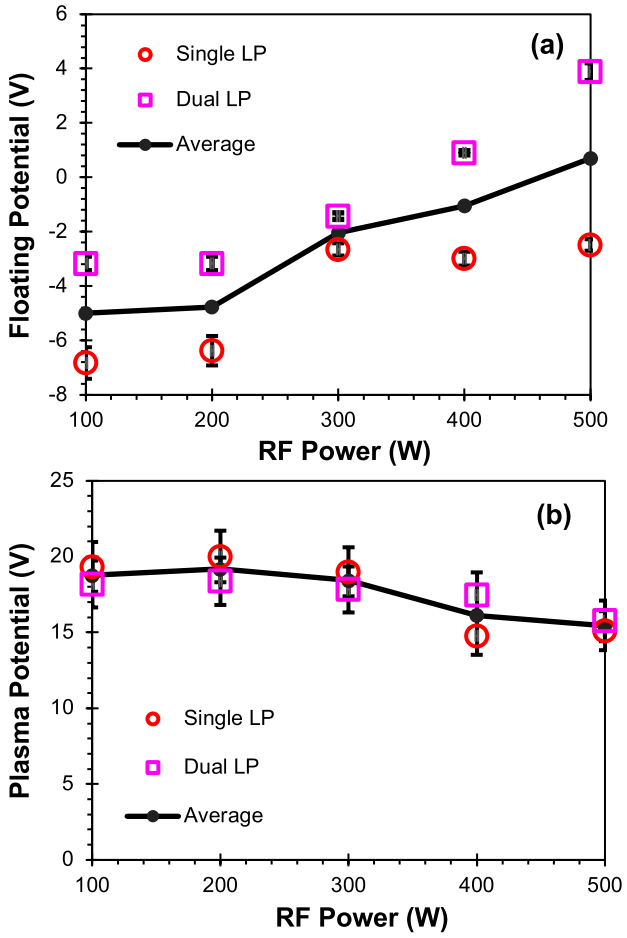

Fig. 11. (a) Floating and (b) plasma potential estimates from single and dual LP data plotted against plasma power.

fits for each power level for both the single [see Fig. 10(a)] and dual [see Fig. 10(b)] LPs. Fig. 11 shows the floating and plasma potentials obtained from the I–V characteristics shown in Fig. 10.

The triple LP gathered two data values: V_{d2} and ion saturation current. Given that the main advantage of a triple LP is its real-time sensing, these two measurements were taken every millisecond for each of the five power levels tested. Due to the quasistatic nature of the measurements conducted by the MLP and the seven different values (listed as the inputs and outputs in Table II) being recorded by the Arduino[1] module on each step, the fastest repetition rate of the measurements was equal to 1 kHz. The V_{d2} measurements were plotted against time for each power level (see Fig. 12). The amplitude of the signals can be seen to decrease linearly with power level, to the point that at 500 W, the signal appears almost constant at 4.2 V. A periodic behavior can also be observed with a frequency of 0.18 Hz for all power levels. To compare the parameters derived from the triple LP data with those obtained from the single and dual LPs, time averages were computed for all the triple LP parameters. The electron temperatures, number densities, and Debye lengths were plotted against the power levels for the single, dual, and triple LPs, and the average of the parameters from all three LP configurations is shown to

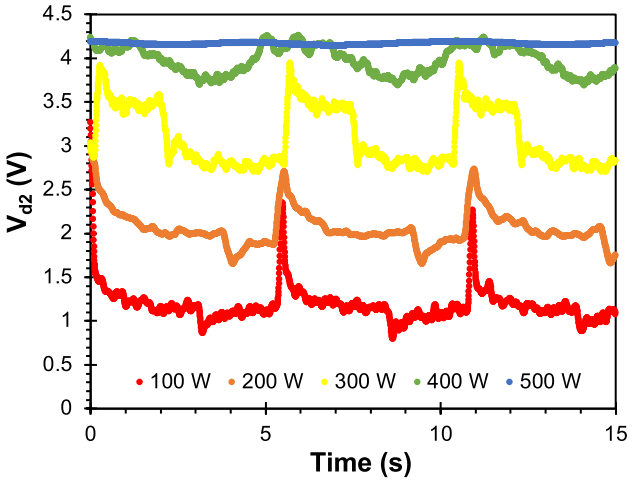

Fig. 12. V_{d2} versus time plots for the triple LP at five RF power levels.

analyze their behavior with respect to plasma RF power (see Fig. 13).

V. Discussion

This study provides a proof-of-concept demonstration of a novel, fully additively manufactured, compact MLP plasma sensor. The device is capable to measure plasma characteristics in both laboratory and ionospheric plasmas (the key factor is the separation of adjacent electrodes—for a given electrode separation, plasmas with a Debye length up to a certain value can be measured without cross-electrode interference). The compact circuitry that runs the MLP is adequate for use on spacecraft that require lightweight and low-power payloads, e.g., CubeSats. The MLP is well within this range, running on 786 mW, weighing only 300 g, occupying 0.29 L, and having an average mass density of 1 kg/L.

As previously discussed, the op-amp array portion of the MLP circuit enabled the voltage outputs from the Arduino[1] modules (which have a lower limit of 0 V) to transform the signal and achieve negative voltages. However, through testing, it was found that an identical op-amp array needed to be implemented for the input signals as well. Therefore, it can be seen in Fig. 10 that any negative input signals (i.e., negative currents for the single and dual LPs) were unable to be measured. These negative values are essential for finding the ion saturation current, which is subsequently used to calculate the number density. Luckily, the triple LP takes a constant measurement of ion saturation current; therefore, this value was able to be substituted into the number density equations for all three LP configurations. However, future iterations of the circuit should rectify this issue by using another op-amp array to the inputs of the MLP circuit.

In Fig. 10(a), slight inflections in the I–V characteristics can be seen at the 300- and 400-W power levels. We believe this is due to the change in mode of the plasma. A helicon plasma can be inductively, capacitively, or wave coupled (H, E, and W modes, respectively); as RF power increases, the helicon plasma shifts from E to H and finally to W mode. The shift in modes from H to W is accompanied

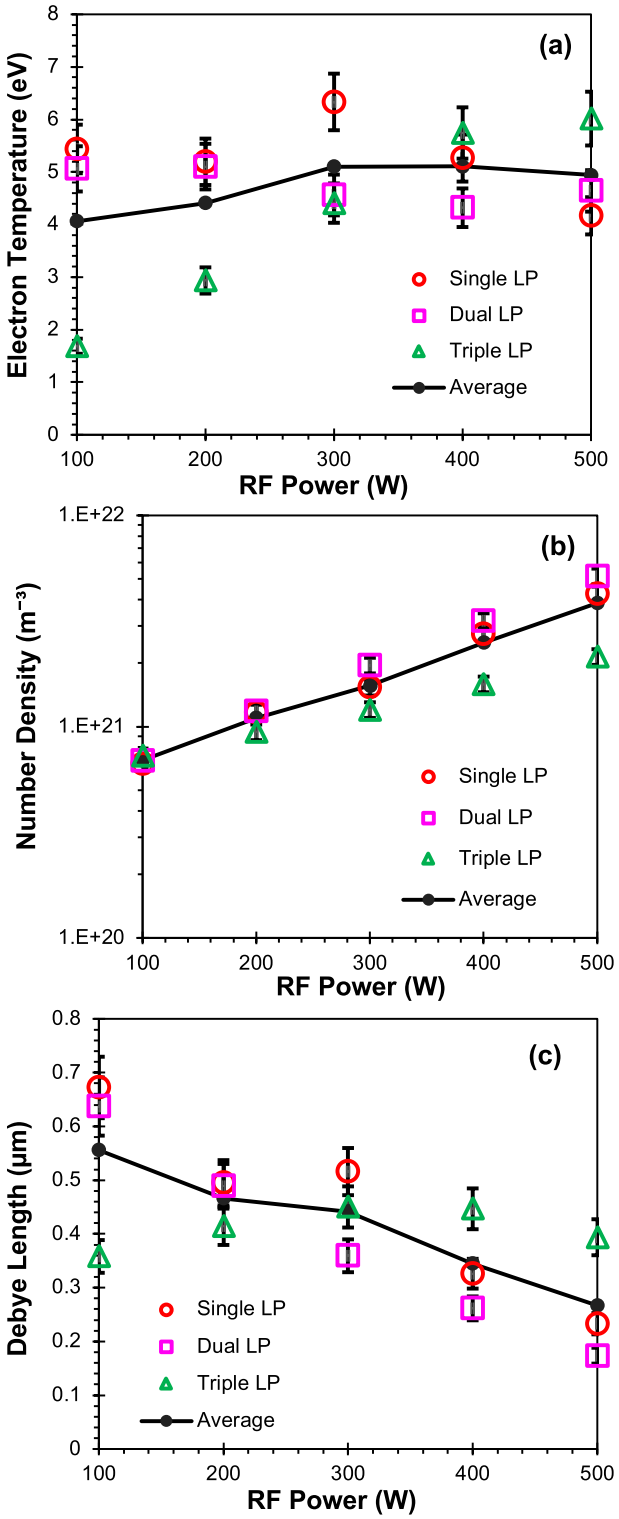

Fig. 13. Time-averaged plasma parameters plotted against power for single, dual, and triple LPs for (a) electron temperature, (b) number density, and (c) Debye length.

by a slight decrease in plasma potential [16]. The fact that the plasma changes from H to W mode as RF power increases is supported by Fig. 11(b), where the plasma potential (which is typically stable over a range of power levels [18]) shows a slight decline in power levels above 300 W. The inflections are only observed in the single LP because it is referenced to an external ground. This represents a good example of the dual LP being better suited to withstand plasma fluctuations.

Fig. 10(a) also shows an inflection at the 500-W power level. This is due to the maximum current being drawn from the electrode (110 μA through a 30-kΩ resistor), resulting in the Arduino[1] module reaching its 3.3 V limit. While this can be addressed by lowering the resistance of the shunt resistor, it should also be noted that this is an example of sheath expansion and a clear demonstration of the dual LPs ability to be resilient to this phenomenon.

The results shown in Fig. 11(a) indicate that the floating potential increases as the RF power increases, which is expected [18] and has been observed in other studies using the same helicon plasma chamber at different power levels [16]. The estimates from the single and dual LPs for both plasma and floating potentials [see Fig. 11(a) and (b), respectively] exhibit excellent agreement. As explained before, triple LPs do not estimate these plasma parameters.

It can be seen in Fig. 13(a) that the electron temperature increases slightly with increasing RF power, which is expected (i.e., as power increases, temperature also increases). The number density is strongly dependent on the plasma RF power [see Fig. 13(b)], with an increase in power resulting in an increase in number density [16]. This relationship also causes the Debye length to be inversely proportional to the RF power, as discussed in Section II-A, which is evident in Fig. 13(c). This range of Debye lengths is low enough to result in r_P/λ_D values greater than 350. Therefore, the assumption made during analysis that the MLP is operating in the thin sheath limit is correct. Also, the separation between adjacent electrodes is much larger than the Debye length, ensuring that the electrodes are not experiencing any interference from one another. If the MLP is used in the ionosphere, the thin sheath limit would not apply, as the Debye length (millimeter scaled) would be far larger than the characteristic width of the electrodes (0.5 mm). Nonetheless, the I–V measurements from the MLP could still be analyzed using the proper framework, e.g., intermediary state, orbital motion limit [8].

The plasma parameters inferred from single and dual LPs are very close, while the estimates from the triple LP are of the same order of magnitude. Nonetheless, the electron temperature from the triple LP significantly lags for low RF power (<300 W), as do the Debye length estimates. This is likely due to the very low measurements of V_{d2}. As discussed previously, the dc bias voltage applied to the triple LP (25 V) should be between five and ten times the value of V_{d2}. This means that any V_{d2} values below 2.5 V are susceptible to sheath expansion and effects from the ratio r_P/λ_D. While the previous values of V_{d2} were in the 3–5 V range, the measurements made here are lower than the 2.5 V cutoff at low power levels below 300 W. This is verified when we plot the maximum value of these parameters from the triple LP in relation to the single and dual LPs (see Fig. 14). These graphs produce significantly better agreement. This clearly highlights that triple LPs are best used for real-time measurements, and time averaging these values does not make a sufficient substitution for other configurations suited to time-averaged values.

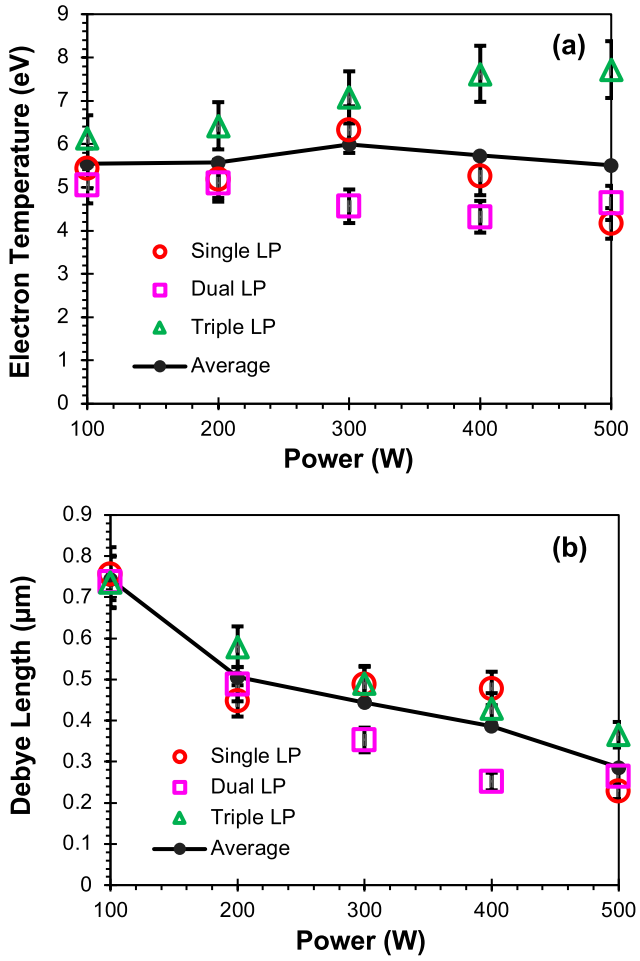

Fig. 14. Single and dual LP time-averaged plasma parameters and maximum values of triple LP plasma parameters plotted against power for (a) electron temperature and (b) Debye length.

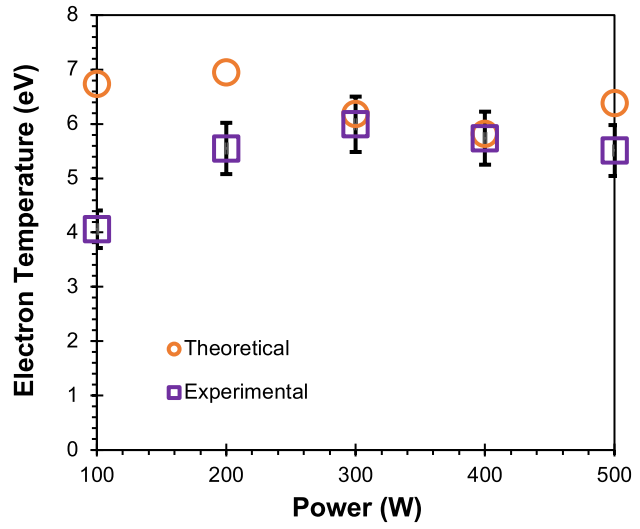

Fig. 15. Theoretical and experimental, LP time-averaged values for electron temperature.

Given that plasmas constantly fluctuate [18], there are no "ground truth" plasma references that can be used to benchmark plasma sensors. Instead, the estimates of plasma parameters are corroborated by measuring in parallel, independently, locally, the same plasma and by comparing the results across the independent estimates. In this study, three different, independent, spatially close LP configurations were run in parallel and the estimated plasma parameters from those measurements are very similar. Furthermore, theoretical values for T_{eV} were calculated by rearranging (2); these values are close to the experimental averages estimated from the MLP data (see Fig. 15). Nonetheless, it should be noted that, in general, the experimental values of T_{eV} are known to be more accurate than the theoretical values [8].

Further improvement of the circuitry could involve using more sensitive components (e.g., microcontrollers, difference amplifiers) with less noise, capable of a larger signal range [33]. These electronics would use a combination of commercial, off the shelf (COTS) and application-specific integrated circuits (ASICs) to attain even lower power consumption, fast response, and high energy efficiency. Given the low ambient temperature in space, it is expected that the electronics have reduced leakage current and less power consumption compared to on-Earth operation. The designs could also be radiation hard through a combination of resilient design techniques, redundancy, and algorithmic error correction [34].

In terms of the 3-D printed hardware, the current version of the MLP reflects the tightest mainstream dimensions and tolerances currently obtainable, and it is a sensor that already complies with the size, weight, and power constraints of a CubeSat. Nonetheless, it might be possible to use artificial intelligence, e.g., generative design to further reduce mass and volume [35]. It might also be possible to use advanced 3-D printing, e.g., micrometallized parts made via two-photon vat polymerization [36], to create even smaller hardware.

VI. Conclusion

This study reported the design, fabrication, and characterization of a compact, MLP that simultaneously operates single, dual, and triple LP configurations to measure plasma parameters with redundancy. The device showcases a compact and energy-efficient design, making it well-suited for implementation on CubeSats to investigate the thermosphere. The utilization of 3-D printing technology facilitated the successful creation of the MLP and makes its construction compatible with in-space manufacturing. The device effectively characterized plasmas within the range of 0.2–0.8-μm Debye lengths. Notably, the electrode separation of the developed MLP sensor enables the examination of plasmas with far larger Debye lengths, extending up to those encountered in the ionosphere. To further enhance its capabilities, a minor adjustment to the circuitry is proposed, which would enable the measurement of negative currents, resulting in capturing data more comprehensively. Other potential improvements in the circuit include the use of COTS, ASICs, and cryogenic operation. The use of more advanced 3-D printing, e.g., micrometallized parts made via two-photon vat polymerization, and the use

of generative design could yield even smaller and lighter hardware.

ACKNOWLEDGMENT

The authors would like to thank Kevin Woller of the Plasma Science and Fusion Center, Department of Nuclear Science and Engineering, Massachusetts Institute of Technology (MIT) for his extensive help in all the experiments done in plasma, and Nathan Rabideaux, Rutgers University, for his help coating the MLP electrodes in iridium.

REFERENCES

[1] B. Zolesi and L. R. Cander, "The general structure of the ionosphere," in *Ionospheric Prediction and Forecasting*, 1st ed. New York, NY, USA: Springer-Verlag, 2014, pp. 11–48.

[2] S. C. Solomon, H. Liu, D. R. Marsh, J. M. McInerney, L. Qian, and F. M. Vitt, "Whole atmosphere simulation of anthropogenic climate change," *Geophys. Res. Lett.*, vol. 45, no. 3, pp. 1567–1576, Feb. 2018, doi: 10.1002/2017gl076950.

[3] T. M. Roberts, K. A. Lynch, R. E. Clayton, J. Weiss, and D. L. Hampton, "A small spacecraft for multipoint measurement of ionospheric plasma," *Rev. Sci. Instrum.*, vol. 88, no. 7, Jul. 2017, Art. no. 073507, doi: 10.1063/1.4992022.

[4] H. W. Jones, "The recent large reduction in space launch cost," in *Proc. 48th Int. Conf. Environ. Syst.*, Albuquerque, NM, USA, 2018, pp. 1–10.

[5] R. A. de Carvalho, *Nanosatellites: Space and Ground Technologies, Operations and Economics*. Hoboken, NJ, USA: Wiley, 2020.

[6] L. F. Velásquez-García, J. Izquierdo-Reyes, and H. Kim, "Review of in-space plasma diagnostics for studying the Earth's ionosphere," *J. Phys. D, Appl. Phys.*, vol. 55, no. 26, Feb. 2022, Art. no. 263001, doi: 10.1088/1361-6463/ac520a.

[7] R. B. Lobbia and A. D. Gallimore, "High-speed dual Langmuir probe," *Rev. Sci. Instrum.*, vol. 81, no. 7, Jul. 2010, Art. no. 073503, doi: 10.1063/1.3455201.

[8] R. B. Lobbia and B. E. Beal, "Recommended practice for use of Langmuir probes in electric propulsion testing," *J. Propuls. Power*, vol. 33, no. 3, pp. 566–581, May 2017, doi: 10.2514/1.b35531.

[9] A. Qayyum, N. Ahmad, S. Ahmad, F. Deeba, R. Ali, and S. Hussain, "Time-resolved measurement of plasma parameters by means of triple probe," *Rev. Sci. Instrum.*, vol. 84, no. 12, Dec. 2013, Art. no. 123502, doi: 10.1063/1.4838658.

[10] E. F. C. Chimamkpam, E. S. Field, A. I. Akinwande, and L. F. Velásquez-García, "Resilient batch-fabricated planar arrays of miniaturized Langmuir probes for real-time measurement of plasma potential fluctuations in the HF to microwave frequency range," *J. Microelectromech. Syst.*, vol. 23, no. 5, pp. 1131–1140, Oct. 2014, doi: 10.1109/JMEMS.2014.2306631.

[11] S. Ghosh, K. K. Barada, P. K. Chattopadhyay, J. Ghosh, and D. Bora, "Resolving an anomaly in electron temperature measurement using double and triple Langmuir probes," *Plasma Sources Sci. Technol.*, vol. 24, no. 1, Dec. 2014, Art. no. 015017, doi: 10.1088/0963-0252/24/1/015017.

[12] W. Jin et al., "Multi-mode Langmuir probe three-in-one detection system and detection method," E.U. Patent CN 202 210 833 109, Sep. 27, 2022.

[13] J. Izquierdo-Reyes, Z. Bigelow, N. K. Lubinsky, and L. F. Velásquez-García, "Compact retarding potential analyzers enabled by glass-ceramic vat polymerization for CubeSat and laboratory plasma diagnostics," *Additive Manuf.*, vol. 58, Oct. 2022, Art. no. 103034, doi: 10.1016/j.addma.2022.103034.

[14] D. V. M. Máximo and L. F. Velásquez-García, "Additively manufactured electrohydrodynamic ionic liquid pure-ion sources for nanosatellite propulsion," *Additive Manuf.*, vol. 36, Dec. 2020, Art. no. 101719, doi: 10.1016/j.addma.2020.101719.

[15] C. K. Tsui, J. A. Boedo, P. C. Stangeby, and T. Team, "Accounting for Debye sheath expansion for proud Langmuir probes in magnetic confinement fusion plasmas," *Rev. Sci. Instrum.*, vol. 89, no. 1, Jan. 2018, Art. no. 013505, doi: 10.1063/1.4995353.

[16] K. B. Woller, D. G. Whyte, and G. M. Wright, "Broad ion energy distributions in helicon wave-coupled helium plasma," *Phys. Plasmas*, vol. 24, no. 5, pp. 1–26, May 2017, doi: 10.1063/1.4983315.

[17] J.-S. Chang and J. G. Laframboise, "Double-probe theory for a continuum low-density plasma," *J. Phys. D, Appl. Phys.*, vol. 9, no. 12, pp. 1699–1703, Aug. 1976, doi: 10.1088/0022-3727/9/12/008.

[18] F. Chen, "Lecture notes on Langmuir probe diagnostics," in *Proc. IEEE-ICOPS Meeting*, Jeju-si, South Korea, Jun. 2003.

[19] K. S. Lay, L. Li, and M. Okutsu, "High altitude balloon testing of Arduino and environmental sensors for CubeSat prototype," *HardwareX*, vol. 12, Oct. 2022, Art. no. e00329, doi: 10.1016/j.ohx.2022.e00329.

[20] T. P. Reynolds et al., "SOC-I: A CubeSat demonstration of optimization-based real-time constrained attitude control," in *Proc. IEEE Aerosp. Conf.*, Big Sky, MT, USA, Mar. 2021, pp. 1–18, doi: 10.1109/AERO50100.2021.9438540.

[21] A. Roman-Gonzalez, A. E. Quiroz-Olivares, and N. I. Vargas-Cuentas, "Advances in the UCHSat-1 nanosatellite: Design and simulation," *Adv. Astronaut. Sci. Technol.*, vol. 3, no. 1, pp. 65–74, Jun. 2020, doi: 10.1007/s42423-020-00054-1.

[22] A. Poghosyan and A. Golkar, "CubeSat evolution: Analyzing CubeSat capabilities for conducting science missions," *Prog. Aerosp. Sci.*, vol. 88, pp. 59–83, Jan. 2017, doi: 10.1016/j.paerosci.2016.11.002.

[23] *Small Spacecraft Technology State of the Art*, Standard TP-2015-216648/REV1, NASA, 2015.

[24] K. Sathish et al., "A comparative study on subtractive manufacturing and additive manufacturing," *Adv. Mater. Sci. Eng.*, vol. 2022, pp. 1–8, Apr. 2022, doi: 10.1155/2022/6892641.

[25] J. I. Samaniego, X. Wang, L. Andersson, D. Malaspina, R. E. Ergun, and M. Horányi, "Investigation of coatings for Langmuir probes in an oxygen-rich space environment," *J. Geophys. Res., Space Phys.*, vol. 123, no. 7, pp. 6054–6064, Jul. 2018, doi: 10.1029/2018ja025563.

[26] Z. Sun, G. Vladimirov, E. Nikolaev, and L. F. Velásquez-García, "Exploration of metal 3-D printing technologies for the microfabrication of freeform, finely featured, mesoscaled structures," *J. Microelectromech. Syst.*, vol. 27, no. 6, pp. 1171–1185, Dec. 2018, doi: 10.1109/JMEMS.2018.2875158.

[27] L. F. Velásquez-García and Y. Kornbluth, "Biomedical applications of metal 3D printing," *Annu. Rev. Biomed. Eng.*, vol. 23, no. 1, pp. 307–338, Jul. 2021, doi: 10.1146/annurev-bioeng-082020-032402.

[28] R. E. Ergun et al., "Dayside electron temperature and density profiles at Mars: First results from the MAVEN Langmuir probe and waves instrument," *Geophys. Res. Lett.*, vol. 42, no. 21, pp. 8846–8853, Nov. 2015, doi: 10.1002/2015gl065280.

[29] C. S. Fish et al., "Design, development, implementation, and on-orbit performance of the dynamic ionosphere CubeSat experiment mission," *Space Sci. Rev.*, vol. 181, nos. 1–4, pp. 61–120, Feb. 2014, doi: 10.1007/s11214-014-0034-x.

[30] M. Dadkhah, J.-M. Tulliani, A. Saboori, and L. Iuliano, "Additive manufacturing of ceramics: Advances, challenges, and outlook," *J. Eur. Ceram. Soc.*, vol. 43, no. 15, pp. 6635–6664, Dec. 2023.

[31] L. Fanelli et al., "A versatile retarding potential analyzer for nanosatellite platforms," *Rev. Sci. Instrum.*, vol. 86, no. 12, Dec. 2015, Art. no. 124501, doi: 10.1063/1.4937622.

[32] A. Edpuganti, V. Khadkikar, M. S. E. Moursi, H. Zeineldin, N. Al-Sayari, and K. Al Hosani, "A comprehensive review on CubeSat electrical power system architectures," *IEEE Trans. Power Electron.*, vol. 37, no. 3, pp. 3161–3177, Mar. 2022, doi: 10.1109/TPEL.2021.3110002.

[33] S. N. Andreev, A. V. Bernatskiy, and V. N. Ochkin, "Increasing the measurement range of plasma electron parameters in the single Langmuir probe method," *Bull. Lebedev Phys. Inst.*, vol. 47, no. 10, pp. 317–319, Oct. 2020, doi: 10.3103/s1068335620100024.

[34] Z. Gao et al., "Fault tolerant parallel FFTs using error correction codes and Parseval checks," *IEEE Trans. Very Large Scale Integr. (VLSI) Syst.*, vol. 24, no. 2, pp. 769–773, Feb. 2016, doi: 10.1109/TVLSI.2015.2408621.

[35] Z. Jiang, H. Wen, F. Han, Y. Tang, and Y. Xiong, "Data-driven generative design for mass customization: A case study," *Adv. Eng. Informat.*, vol. 54, Oct. 2022, Art. no. 101786, doi: 10.1016/j.aei.2022.101786.

[36] F. Zhang et al., "The recent development of vat photopolymerization: A review," *Additive Manuf.*, vol. 48, Dec. 2021, Art. no. 102423, doi: 10.1016/j.addma.2021.102423.

Zoey Bigelow received the B.Sc. degree in electrical engineering from the University of Alaska Anchorage, Anchorage, AK, USA, in 2021, and the master's degree in electrical engineering from Massachusetts Institute of Technology (MIT), Cambridge, MA, USA, in 2023, where he is currently pursuing the Ph.D. degree.

His research interests include plasma sensor technology and pioneering additive manufacturing techniques.

Luis Fernando Velásquez-García (Senior Member, IEEE) received the Mechanical Engineer and Civil Engineer degrees (magna cum laude and valedictorian of the School of Engineering in both cases) from the Universidad de Los Andes, Bogotá, Colombia, in 1998 and 1999, respectively, and the M.S. and Ph.D. degrees from Massachusetts Institute of Technology (MIT), Cambridge, MA, USA, in 2001 and 2004, respectively.

In 2004, after completing his studies, he became a Post-Doctoral Associate with the Microsystems Technology Laboratories (MTL), MIT, where he was appointed as a Research Scientist, in 2005. Since 2009, he has been a Principal Scientist and Core Member with MTL. He is an expert in micro and nanofabrication technologies. He leads the Micro- and Nano-enabled Multiplexed Scaled-down Systems Group at MIT, which conducts fundamental and applied research on miniaturized devices and systems that exploit high-electric field phenomena (e.g., electrospray, gas ionization, field emission, X-rays, and plasmas) for space, energy, healthcare, manufacturing, and analytical applications. He has authored more than 66 journal publications and 103 conference proceedings publications, and he holds 16 patents on nanoelectromechanical systems (NEMS)/microelectromechanical systems (MEMS) technologies. His work currently focuses on additively manufactured micro and nanosystems.

Dr. Velásquez-García is a full member of Sigma Xi and a senior member of the American Institute of Aeronautics and Astronautics (AIAA). His group's work has received multiple recognitions, including best paper awards in conferences, such as PowerMEMS and Transducers, and best-paper highlights at journals, such as the IEEE JOURNAL OF MICROELECTROMECHANICAL SYSTEMS, the *IOP Journal of Physics D: Applied Physics*, the *IOP Journal of Micromechanics and Microengineering*, and *IOP Nanotechnology*. He served as the Co-Chair of the 15th International Conference on Micro and Nanotechnology for Power Generation and Energy Conversion Applications (PowerMEMS 2015) and as the Chair of the 36th International Vacuum Nanoelectronics Conference (IVNC 2023). He is currently the Vice President of Finance of the IEEE MEMS Technical Community.